Ivan Rýger

Autoreferát dizertačnej práce

AlGaN/GaN BASED HIGH ELECTRON MOBILITY TRANSISTORS AND SURFACE ACOUSTIC WAVES FOR HYDROGEN SENSING

na získanie   akademickej hodnosti doktor (philosophiae doctor, PhD.)

v doktorandskom študijnom programe: Mikroelektronika

v študijnom odbore   5.2.13 Mikroelektronika

Miesto a dátum: Bratislava 2.7.2015

Dizertačná práca bola vypracovaná v dennej forme doktorandského štúdia

Na   Elektrotechnickom ústave Slovenskej akadémie vied

Dúbravská cesta 9, 841 04 Bratislava

Predkladateľ: Ing. Ivan Rýger, Elektrotechnický ústav SAV

Dúbravská cesta 9, 841 04 Bratislava

Školiteľ: Ing. Tibor Lalinský, DrSc., Elektrotechnický ústav SAV

Dúbravská cesta 9, 841 04 Bratislava

Oponenti:

Autoreferát bol rozoslaný: ....

Obhajoba dizertačnej práce sa koná: ....

Na   ....

Prof. Dr. Ing. Miloš Oravec
Dekan FEI STU v Bratislave
Ilkovičova 3, 812 19 Bratislava

Contents

Anotácia

Táto dizertačná práca je venovaná aplikácii nitridu gália (GaN) pre senzory plynov. Vyšetrované sú dva nezávislé princípy snímania plynov, ktoré umožňujú snímanie v sťažených podmienkach. Prvý-čisto elektronický a druhý, elektro-akustický.

Prvá časť práce je venovaná štúdiu princípu činnosti plynových senzorov na báze Schottkyho diód a tranzistorov s vysokou pohyblivosťou elektrónov (High Electron Mobility Transistor - HEMT). Študovaný je reakčný mechanizmus a chemická reakčná kinetika prebiehajúca v procese snímania týchto senzorov. Experimentálna časť tejto práce popisuje návrh a vlastnosti senzorov vodíka na báze AlGaN/GaN HEMT snímacích prvkov. Tento senzor využíva nanokryštalické dvojvrstvy Pt/NiO a Pt/IrO$_2$ ako hradlové elektródy tranzistorov. Študovali sme ako nanokryštalická štruktúra zmienených vrstiev ovplyvňuje absorpciu vodíka ako aj elektrické transportné vlastnosti hradlových rozhraní. Následne sme vyšetrovali vplyv hrúbky hradlových oxidových vrstiev na detekčné vlastnosti senzorov. Schottkyho dióda s 20 nm hrubou optimalizovanou vrstvou NiO vykazovala 60-násobný nárast v citlivosti v porovnaní s diódou na báze jednoduchej hradlovej katalytickej vrstvy Pt (Pt/AlGaN/GaN). Tento efekt môže byť vysvetlený efektívnejšou disociáciou vodíkových molekúl na povrchu nanokryštalickej Pt/NiO dvojvrstvy. Ukázali sme taktiež, že optimálna pracovná teplota senzora bola posunutá z 250°C (referenčný Pt/AlGaN/GaN senzor) na 50°C (senzor s NiO).

Druhá časť tejto dizertačnej práce je venovaná senzorom vodíka na báze povrchových akustických vĺn (Surface Acoustic Waves- SAW). Opäť, v teoretickom úvode sme študovali princíp činnosti takýchto senzorov. Prezentujeme aplikáciu epitaxných GaN vrstiev rastených na SiC pre SAW senzor vodíka so zvýšenou citlivosťou a popisujeme ich technológiu prípravy. Následne sú tieto štruktúry merané a z nich sú stanovené určené základné fyzikálno-akustické parametre epitaxných vrstiev a vrchných metalizačných vrstiev. Z meraní sme stanovili ako fázovú, tak i skupinovú rýchlosť a efektívny koeficient elektro-mechanickej väzby v daných štruktúrach ako funkciu vlnovej dĺžky SAW. Študovali sme jej vplyv a vplyv vybudených vyšších módov Rayleigho vlny na citlivosť senzora v dôsledku zaťaženia hmotnosťou (mass-loading effect). Ukázali sme, že vplyv tohto efektu môže byť zvýšený skrátením akustickej vlnovej dĺžky a sústredením elastickej energie do epitaxného GaN vlnovodu. Cieľom bolo navrhnúť mikrovlnný SAW oscilátor na princípe oneskorovacej linky so zvýšenou citlivosťou, ktorého parametre sme následne analyzovali. Posuv frekvencie oscilátora bol viac než 60kHz po aplikovaní zmesi 1000 ppm H$_2$/N$_2$ pri izbovej teplote. Reakčný čas senzora pri rovnakých podmienkach bol 12 s. Frekvenčný posuv oscilátora ukazuje lineárnu závislosť na koncentrácii vodíka. Toto je výhoda využiteľná pri plynových analyzátoroch.

Abstract

In this dissertation we are dealing with application of gallium nitride (GaN) material for gas sensors. Two independent gas sensing principles offering the capability of harsh conditions sensing are investigated. The first is purely electronic and the second is electroacoustic.

In the first part of this dissertation, we studied the theoretical background of Schottky diode and High Electron Mobility Transistor (HEMT)-based gas sensors. The reaction mechanism and kinetics are described, as well. The experimental part reports on the design and performance of a hydrogen sensor based on AlGaN/GaN Circular HEMT. This sensor uses hydrogen-sensitive nanocrystalline Pt/NiO or Pt/IrO$_2$ stacked layer as a gate electrode. We investigated how the hydrogen absorption properties of the sensor are influenced by the nanocrystalline structure of these layers. We analyzed the electrical properties of this interface and studied the sensory performance of such Schottky gate diode sensors to hydrogen versus the varied thickness of the oxide layers. The diode based on optimized 20 nm thick NiO interlayer exhibited a 60-fold increase in sensitivity compared with that of a conventional Pt/AlGaN/GaN diode sensor. This can be explained considering that hydrogen dissociated more efficiently at the nanocrystalline surface of the Pt/NiO stack. We show that the optimal operation temperature of the sensor shifted considerably from 250 °C (reference Pt/AlGaN/GaN sensor) to as low as 50 °C (sensor with the NiO layer).

The second part of this dissertation is dedicated to surface acoustic wave-based hydrogen sensors. Again, in the theoretical introduction, the sensory mechanism is described. Then we present an application of epitaxial GaN layers grown on SiC substrates for Surface Acoustic Wave (SAW) hydrogen sensors with enhanced sensitivity also describing the sensor fabrication process. Next, the electrical properties of the sensors are measured and then the basic acoustic quantities of epitaxial films and metallic gratings are extracted. The SAW wavelength-dependent phase and group velocity and electromechanical coupling factors were determined. We investigate the effect of wavelength and excitation mode on the mass sensitivity of the proposed sensor. We demonstrate that the mass-loading sensitivity of such sensors can be increased by using shorter acoustic wavelengths and by confining the acoustic wave energy in an epitaxial GaN waveguide. The effect of different Rayleigh-like modes on the mass-loading sensitivity is also discussed. The outcome was used to design a microwave SAW delay-line oscillator. We finally demonstrate a prototype of a sensor based on a microwave SAW delay line oscillator with improved sensing response. Its sensing characteristics are presented. The oscillator frequency shift was larger than 60 kHz after exposure to 1000 ppm H$_2$/N$_2$ at room temperature. The sensor reaction time was about 12 s for the same sensing conditions. The oscillator frequency shift shows linear dependence on hydrogen concentration frequency shift. This is particular advantage for gas analytic systems.

8   List of Author's citations

Vanko, G., Hudek, P., Dzuba, J., Choleva, P., Kutiš, V., Vallo, M., Rýger, I., Lalinský, T., : Bulk micromachining of SiC substrate for MEMS sensor applications. Microelectron. Engn. 110 (2013) 260-264.
    1. Olhero, S. M.: Mater. Research Bull. 60 (2014) 830.
    2. Preusch, F.: Micromachines 5 (2014) 1051.
    3. Leclaire, P.: Semicond. Sci Technol. 29 (2014) 115018.
\#   4. Frischmuth, T.: Procedia Engn. 87 (2014) 128.

Vallo, M., Lalinský, T., Dobročka, E., Vanko, G., Vincze, A., Rýger, I., : Impact of Ir gate interfacial oxide layers on performance of AlGaN/GaN HEMT,. Applied Surface Sci 267 (2013) 159-163.
    1. Lin, R.-M.: Japan. J. Applied Phys. 52 (2013) 111002.

Lalinský, T., Vanko, G., Vallo, M., Dobročka, E., Rýger, I., Vincze, A., : AlGaN/GaN high electron mobility transistors with nickel oxide based gates formed by high temperature oxidation. Applied Phys. Lett. 100 (2012) 092105.
    1. Liu, H.-Y.: IEEE Trans. Electron Dev. 60 (2013) 2231.
    2. Kawakami, R.: Japan. J. Applied Phys. 52 (2013) SIUNSP05EC05.
    3. Binh, T.T.: Electronic Mater. Lett. 9 (2013) 705.
    4. Harmatha, L.: Applied Surface Sci 312 (2014) 102.

Vanko, G., Držík, M., Vallo, M., Lalinský, T., Kutiš, V., Stančík, S., Rýger, I., Benčurová, A., : AlGaN/GaN C-HEMT structures for dynamic stress detection. Sensors Actuators A 172 (2011) 98-102.
    1. Wang, A.: IEEE Trans. Electron Dev. 60 (2013) SI3149.

Lalinský, T., Vanko, G., Vallo, M., Držík, M., Bruncko, J., Jakovenko, J., Kutiš, V., Rýger, I., Haščík, Š., Husák, M., : Impact of ZnO gate interfacial layer on piezoelectric response of AlGaN/GaN C-HEMT based ring gate capacitor. Sensors Actuators A 172 (2011) 386-391
    1. Wang C.: Chinese Phys. Lett. 31 (2014) 128501.

Vanko, G., Lalinský, T., Haščík, Š., Rýger, I., Mozolová, Ž., Škriniarová, J., Tomáška, M., Kostič, I., Vincze, A., : Impact of SF6 plasma treatment on performance of AlGaN/GaN HEMT. Vacuum 84 (2009) 235-237.
    1. Wang, Y.Z.: Applied Phys. Lett. 98 (2011) 043506.
    2. Hirose, M.: Phys. Status Solidi C 9 (2012) 361.
    3. Wang, Y.Z.: Applied Phys. Lett. 101 (2012) 063505.
    4. Zhang, H.Y.: J. Phys. D 46 (2013) 435102.
    5. Bisi, D.: Europ. Solid-State Dev. Research Conf. 2013, Art. no. 6818819, P. 61.
    6. Lee, N.-H.: Japan. J. Applied Phys. 53 (2014) SI04EF10.
    7. Du, Y.-D.: Chinese Phys. Lett. 31 (2014) 048501.

Lalinský, T., Rýger, I., Rufer, L., Vanko, G., Haščík, Š., Mozolová, Ž., Škriniarová, J., Tomáška, M., Kostič, I., Vincze, A., : Surface acoustic wave excitation on SF6 plasma-treated AlGaN/GaN heterostructure. Vacuum 84 (2009) 231-234.
    1. Zhang, D.: Materials Research Bull. 46 (2011) 1582.

Dzuba, J., Lalinský, T., Vanko, G., Vallo, M., Rýger, I., Kutiš, V., Královič, V., : Modeling and simulation of AlGaN/GaN piezoelectric MEMS pressure sensor. In: 13th Mechatronics Forum Inter. Conf. – Mechatronics 2012. Linz 2012. P. 773-778.

2011

Rýger, I., Vanko, G., Lalinský, T., Vallo, M., Tomáška, M., Ritomský, A., : AlGaN/GaN based SAW-HEMT devices for chemical gas sensors operating in GHz range. Procedia Engn. 25 (2011) 1101-1104.

Vanko, G., Držík, M., Vallo, M., Lalinský, T., Kutiš, V., Stančík, S., Rýger, I., Benčurová, A., : AlGaN/GaN C-HEMT structures for dynamic stress detection. Sensors Actuators A 172 (2011) 98-102

Lalinský, T., Vanko, G., Vallo, M., Držík, M., Bruncko, J., Jakovenko, J., Kutiš, V., Rýger, I., Haščík, Š., Husák, M., : Impact of ZnO gate interfacial layer on piezoelectric response of AlGaN/GaN C-HEMT based ring gate capacitor. Sensors Actuators A 172 (2011) 386-391.

2010

Lalinský, T., Rýger, I., Vanko, G., Tomáška, M., Kostič, I., Haščík, Š., Vallo, M., : AlGaN/GaN based SAW-HEMT structures for chemical gas sensors, Procedia Engn. 5 (2010) 152-155.

Vallo, M., Lalinský, T., Vanko, G., Držík, M., Haščík, Š., Rýger, I., Kostič, I., : AlGaN/GaN C-HEMT for piezoelectric MEMS stress sensor appliocations. In.: MME 2010. Eds. L. Abelmann et al. Enschede: Univ. Twente 2010. ISBN 978-90-816737-1-6. P. 56-59

Vanko, G., Držík, M., Vallo, M., Lalinský, T., Kutiš, V., Stančík, S., Rýger, I., Kostič, I., : AlGaN/GaN C-HEMT structures for dynamic stress detection. Procedia Engn. 5 (2010) 1405-1408.

Rýger, I., Lalinský, T., Vanko, G., Tomáška, M., Kostič, I., Haščík, Š., Vallo, M., : HEMT-SAW structures for chemical gas sensors in harsh environment In: ASDAM '10. Ed. J. Breza et al. Piscataway: IEEE 2010. ISBN: 978-1-4244-8572-7. P. 131-134.

2009

Vanko, G., Lalinský, T., Haščík, Š., Rýger, I., Mozolová, Ž., Škriniarová, J., Tomáška, M., Kostič, I., Vincze, A., : Impact of SF6 plasma treatment on performance of AlGaN/GaN HEMT. Vacuum 84 (2009) 235-237.

Lalinský, T., Rýger, I., Rufer, L., Vanko, G., Haščík, Š., Mozolová, Ž., Škriniarová, J., Tomáška, M., Kostič, I., Vincze, A., : Surface acoustic wave excitation on SF6 plasma-treated AlGaN/GaN heterostructure. Vacuum 84 (2009) 231-234.

2008

Lalinský, T., Rufer, L., Vanko, G., Rýger, I., Haščík, Š., Tomáška, M., Mozolová, Ž., Vincze, A., : Surface acoustic wave excitation on SF6 plasma treated AlGaN/GaN heterostructure. In: ASDAM 2008. Eds. Š. Haščík and J.Osvald. Piscataway: IEEE 2008. ISBN: 978-1-4244-2325-5. P. 311-314.

1 Introduction

Gas sensors are the topic of tremendous scientific research because of wide range of applications from environmental monitoring, chemical and food industry, nuclear plant safety up to common household appliances. This opens a great sensor market opportunities. Especially, the sensors for demanding environmental conditions are needed.

Conventional silicon-based sensors are not capable of operation at elevated temperature due to low energy band gap of this semiconductor material, resulting in low intrinsic temperature. Group III-nitrides [1] seem to be promising candidates for high-temperature operating electronic circuits. We have chosen the gallium nitride as the topic of scientific research due to its large energy band gap (3.4 eV)[2], stability of its mechanical properties at elevated temperature and inherent piezoelectric properties. In the case of compound semiconductors (as AlGaN/GaN heterostructure) the 2 dimensional electron gas (2DEG) is being formed at the hetero-interface. This channel is in the case of AlGaN/GaN heterostructure induced by spontaneous and piezoelectric polarization [3] and is sensitive to surface states. This is great advantage in sensor applications [4]. Moreover, a stable hydrogen chemical sensor based on AlGaN/GaN HEMT was demonstrated in literature [5]. Additionally, the stability of GaN material parameters allows the construction of micro electro mechanical system (MEMS) sensors employing mechanical detection principle, what excludes the need of electronic components that are instable at high temperature. The SAW-based chemical sensors fabricated on AlGaN/GaN heterostructure material offers the possibility of high temperature operation provided that the direct interaction of forcing electromagnetic wave with 2DEG channel is suppressed [6]. In previous work, we focused on demonstration of surface acoustic wave (SAW) based chemical sensors using microwave oscillator [7],[8].

2 Background

2.1 HEMT Schottky gate hydrogen sensors

The hydrogen sensor based on Metal-oxide-semiconductor was published for the first time by Lundström et al. [9]. Authors have showed that if the catalytic metal is deposited on top of MOS transistor, the hydrogen molecules are split into atoms that are subsequently ionized and allow the creation of dipolar layer on the transistor gate interface. Consequently, the threshold voltage is altered, what leads to transistor drain current change at fixed bias voltage. This idea was then adapted also to rectifying Schottky metal-semiconductor contacts. In the case of AlGaN/GaN heterostructure-based Schottky diode sensors (Fig. 2.1), it is speculated that hydrogen atoms can bind to unsaturated chemical bonds (states) on AlGaN surface and therefore they create polar bonds. Consequently the effective Schottky barrier height lowering is observed [10],[11].
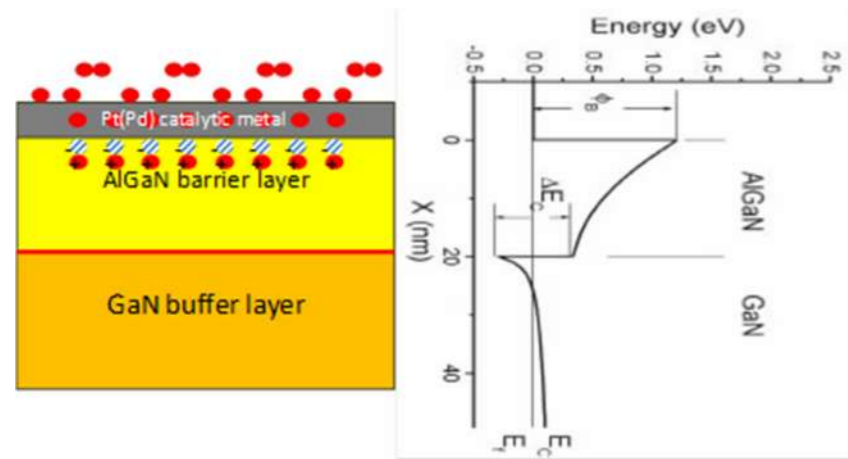
Fig. 2.1. AlGaN/GaN based Schottky diode sensor and its corresponding energy band diagram.

Matsuo, K. et al. [12] using the thin surface barrier model [13] shows that the hydrogen induced Schottky barrier lowering in the case of Pt/AlGaN/GaN Schottky barrier diode sensor can be affected either by formation of hydrogen-induced dipole at M-S interface or to hydrogen passivation of surface states causing Fermi level pinning at the M-S interface. He supported the measured data by computer simulations. Additionally, the two dimensional electron gas induced by spontaneous and piezoelectric polarization on AlGaN/GaN interface (Fig. 2.1) is very sensitive to the concentration of surface states. This led to the excellent sensing characteristics of a Pt/AlGaN/GaN HEMT transistor at 600°C, about which Song, J. et al. reported [5].

2.2 SAW sensors working principle

Unlike semiconductor-based chemical sensors, these based on the surface acoustic waves employ measurement of acoustic wave physical quantities (phase velocity, attenuation) that are affected by gas sensing film. The main advantage of such sensors is that mechanical and piezoelectric properties of these materials (such as GaN, Langasite) are more stable in wide temperature range than the electronic properties of semiconductors.

Surface acoustic waves in general can be employed for sensors or thin-film characterization, as the acoustic strain energy is concentrated in surface vicinity. The measured response arises from perturbation in wave propagation. Provided that piezoelectric materials are usually employed to generate this kind of wave, both mechanical and electrical coupling between the SAW and surface film are possible. A number of interactions between SAW and thin-film give rise to velocity and attenuation response [14], pp.78.

1   Mass-loading effect caused by mechanical coupling between crystal surface and thin film. It is caused by translation of surface mass by SAW displacement.

2   The elastic and visco-elastic effects are caused by SAW induced mechanical strain in surface film.

3   The acousto-electric interaction arises from electrical coupling between the SAW and conductive film.

škola vákuovej techniky. Eds. M. Vojs, M. Veselý. Bratislava: Slov. vákuová spol. 2013. ISBN 978-80-971179-2-4. S. 55-59.

Vanko, G., Hudek, P., Dzuba, J., Choleva, P., Kutiš, V., Vallo, M., Rýger, I., Lalinský, T., : Bulk micromachining of SiC substrate for MEMS sensor applications. Microelectron. Engn. 110 (2013) 260-264.

Vallo, M., Lalinský, T., Dobročka, E., Vanko, G., Vincze, A., Rýger, I., : Impact of Ir gate interfacial oxide layers on performance of AlGaN/GaN HEMT,. Applied Surface Sci 267 (2013) 159-163.

Lalinský, T., Vallo, M., Vanko, G., Dobročka, E., Vincze, A., Osvald, J., Rýger, I., Dzuba, J., : Iridium oxides based gate interface of AlGaN/GaN high electron mobility transistors formed by high temperature oxidation. Applied Surface Sci 283 (2013) 160-167.

Vanko, G., Hudek, P., Zehetner, J., Dzuba, J., Choleva, P., Vallo, M., Rýger, I., Lalinský, T., : MEMS pressure sensor fabricated by advanced bulk micromachining techniques, Proc. SPIE 8763 (2013) 8763-101.

Kutiš, V., Gálik, G., Rýger, I., Paulech, J., Murín, J., Hrabovský, J., Lalinský, T., : Modal and transient analysis of SAW MEMS sensor. In: Proc. 19th Inter. Conf. on Applied Phys. of Cond. Matter (APCOM 2013). Eds. J. Vajda and I. Jamnický. Bratislava: FEI STU 2013. ISBN 978-80-227-3956-6. P. 221-224.

Vincze, A., Vallo, M., Dobročka, E., Rýger, I., Vanko, G., Lalinský, T., : SIMS and XRD analysis on Ir contact layers for AlGaN/GaN HEMT structures. In: Proc. ADEPT. 1st Inter. Conf. on Advan. in Electronic and Photonic Technol. Eds. D. Pudis et al. Žilina: Univ. Žilina 2013. ISBN 978-80-554-0689-3. P. 295-298.

2012

Rýger, I., Vanko, G., Kunzo, P., Lalinský, T., Vallo, M., Plecenik, A., Satrapinskyy, L., Plecenik, T., :AlGaN/GaN HEMT based hydrogen sensors with gate absorption layers formed by high temperature oxidation. Procedia Engn. 47 (2012) 518-521.

Lalinský, T., Vanko, G., Vallo, M., Dobročka, E., Rýger, I., Vincze, A., : AlGaN/GaN high electron mobility transistors with nickel oxide based gates formed by high temperature oxidation. Applied Phys. Lett. 100 (2012) 092105.

Rýger, I., Tomáška, M., Vanko, G., Lalinský, T., : An AlGaN/GaN based GHz-range surface acoustic wave oscillator for sensor applications. . In: Proc. 22nd Inter. Conf. Radioelektronika 2012. Eds. R. Balada et al. Brno: Univ. Technol. 2012. ISBN 978-80-214-4468-3. P. 279-282.

Vanko, G., Vallo, M., Rýger, I., Dzuba, J., Lalinský, T., : Conductive metal oxide based gates for self aligned technology of AlGaN/GaN HEMT. In: ASDAM 2012. Eds. Š. Haščík, J. Osvald. Piscataway: IEEE 2012. ISBN 978-1-4673-1195-3. P. 19-22.

Rýger, I., Vanko, G., Kunzo, P., Lalinský, T., Dzuba, J., Vallo, M., Satrapinskyy, L., Plecenik, T., Chvála, A., : Gates of AlGaN/GaN HEMT for high temperature gas sensing applications. In: ASDAM 2012. Eds. Š. Haščík, J. Osvald. Piscataway: IEEE 2012. ISBN 978-1-4673-1195-3. P. 23-26.

7   Author's publications

2015

Rýger. I., Vanko, G., Lalinský, T., Haščík, Š., Benčúrová, A., Nemec, P., Andok, R., Tomáška, M., GaN/SiC based surface acoustic wave structures for hydrogen sensors with enhanced sensitivity, Sensors Actuators A 227 (2015) 55-62.

Dzuba, J., Vanko, G., Držík, M., Rýger, I., Vallo, M., Kutiš, V., Haško, D., Choleva, P., Lalinský, T., : Stress investigation of the AlGaN/GaN micromachined circular diaphragms of a pressure sensor. J. Micromech. Microengn. 25 (2015) 015001.

2014

Vanko, G., Vojs, M., Ižák, T., Potocký, P., Choleva, P., Marton, M., Rýger, I., Dzuba, J., Lalinský, T., : AlGaN/GaN micromembranes with diamond coating for high electron mobility transistors operated at high temperatures In: ASDAM 2014. Eds. J. Breza et al. IEEE 2014. ISBN 978-1-4799-5474-2. P. 263-266.

Rýger, I., Vanko, G., Lalinský, T., Dzuba, J., Vallo, M., Kunzo, P., Vávra, I., : Enhanced sensitivity of Pt/NiO gate based AlGaN/GaN C-HEMT hydrogen sensor Key Engn. Mater. 605 (2014) 491-494.

Dzuba, J., Vanko, G., Rýger, I., Vallo, M., Kutiš, V., Lalinský, T., : Influence of temperature on the sensitivity of the AlGaN/GaN C HEMT based piezoelectric pressure sensor In: ASDAM 2014. Eds. J. Breza et al. IEEE 2014. ISBN 978-1-4799-5474-2. P. 5-8.

Dzuba, J., Držík, M., Vanko, G., Rýger, I., Vallo, M., Kutiš, V., Lalinský, T., : Modal analysis of Gallium Nitride membrane for pressure sensing device Key Engn. Mater. 605 (2014) 404-407.

Vanko, G., Dzuba, J., Rýger, I., Lalinský, T., Vojs, M., Vincze, A., Dobročka, E., : Processing technology of MEMS sensors using III-N material system In: 17. škola vákuovej techniky: Analýza materiálov vo vákuu. Material analysis in vacuum. Eds. M. Michalka et al. Bratislava: FEI STU 2014. ISBN 978-80-971179-4-8. P. 39-43.

Rýger, I., Vanko, G., Lalinský, T., Kunzo, P., Vallo, M., Vávra, I., Plecenik, T., : Pt/NiO ring gate based Schottky diode hydrogen sensors with enhanced sensitivity and thermal stability. Sensors Actuators B 202 (2014) 1-8.

Dzuba, J., Vanko, G., Držík, M., Rýger, I., Vallo, M., Lalinský, T., Kutiš, V., Haško, D., Srnánek, R., : The AlGaN/GaN C-HEMT diaphragm-based MEMS pressure sensor for harsh environment In: 17. škola vákuovej techniky: Analýza materiálov vo vákuu. Material analysis in vacuum. Eds. M. Michalka et al. Bratislava: FEI STU 2014. ISBN 978-80-971179-4-8. P. 142-145.

Zehetner, J., Vanko, G., Choleva, P., Dzuba, J., Rýger, I., Lalinský, T., : Using of laser ablation technique in the processing technology of GaN/SiC based MEMS for extreme conditions In: ASDAM 2014. Eds. J. Breza et al. IEEE 2014. ISBN 978-1-4799-5474-2. P. 259-262.

2013

Vanko, G., Lalinský, T., Ižák, T., Vojs, M., Vincze, A., Dobročka, E., Vallo, M., Dzuba, J., Rýger, I., Kromka, A., : AlGaN/GaN high electron mobility transistors for high temperatures In: Perspektívne vákuové metódy a technológie: 16.

All of these effects result in the change of either wave velocity or attenuation.

The conventional sensor arrangement consists of two interdigital comb transducers (IDT) placed on piezoelectric substrate (Fig. 2.2). The input IDT excites the harmonic sound wave along surface of piezoelectric substrate. This wave is being spread towards output transducer located in right-hand side of this figure, where it is converted back to the electrical signal. A gas sensitive film is located in this propagation path.

The most utilized interaction in sensor systems is based on mass changes on surface of this layer. The particles of crystal surface move about elliptical orbit in synchronism with passing SAW. The additional surface mass binds certain amount of momentum, and thus, the mechanical strain energy. The effect on wave velocity and attenuation can be derived from energy conservation law.

The visco-elastic effect on phase velocity appears, if the gas absorbing layer binds the gas molecules, its mechanical properties (stiffness, mass density) are affected. Consequently, the phase velocity and attenuation is changed in this sensitive film.

In the case of acousto-electrical interaction the SAW propagates in piezoelectric material, so it generates the coupled bound electrostatic charge wave accompanying the mechanical displacement. This bound charge is a source of wave electric potential φ. When a conductive film is deposited on top of piezoelectric medium, the charge carriers move, so that they compensate the external forcing field. The effect of SAW coupled charge carriers accounts for conduction currents in the film and displacement currents in the surrounding dielectric media. The conductive film dissipates certain amout of coupled wave and also affects the energy storage over one signal period. This will result in both wave attenuation and phase velocity change.
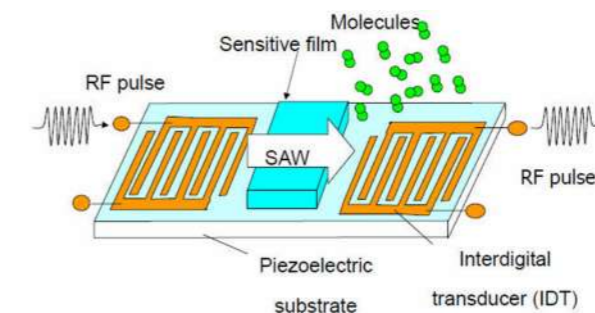

Fig. 2.2. SAW gas sensor topology based on measurement of travelling wave [15].

These changes can be detected in signal processing electronic circuitry. Still, the application of surface-acoustic wave oscillators seems to be the easiest measurement method. Two IDTs are placed in the feedback loop of amplifier [7]. The oscillation frequency of this system (amplifier-SAW filter) is determined by amplitude and phase conditions. The amplitude condition is usually satisfied in relatively wide range of frequencies around IDT transmission peak. The exact oscillation frequency is determined by phase condition that must be integral multiple of 2π. This can be easily satisfied as the usual propagation length is in order of several hundreds of acoustic wavelength. When the phase

shift between two transducers is affected (it is a result of change in the phase velocity), the oscillator frequency at which the phase condition is satisfied will be changed.

3   Research objectives

In this dissertation I will:

1. Gain a new knowledge from the field of AlGaN/GaN-based hydrogen senors. These devices should be capable of operation in harsh conditions (high temperature, corrosive environment).

2. Design and test the concept of two compatible sensing principles: the first based on High Electron Mobility Transistors (HEMT) and the second based on Surface Acoustic Waves (SAW).

3. Design the modified gate hydrogen absorbing layer that could be used in AlGaN/GaN-based C-HEMT hydrogen sensor. This layer should allow the hydrogen sensing with increased sensitivity at relatively low working temperature.

4. Contribute to the determination of HEMT-based sensor hydrogen detection model. This should be done by analysis of sensor response at varying temperature together with microstructure and chemical analysis of gate absorption layer.

5. Design SAW-structures using GaN/SiC material system. These structures should suppress undesirable acoustic wave reflections and allow the measurement of physical quantities of excited acoustic waves.

6. Elaboration of measurement method for phase velocity and effective electro-mechanical coupling factor determination for above mentioned piezoelectric material system.

7. Design and test the SAW-based hydrogen sensor concept. Contribute to detection model identification by investigation of sensor detection properties.

4   Summary of achieved results

In the first part of this dissertation, we focused our attention to gas sensors based on HEMT gate schottky junction, we investigated the effect of additional metal oxide layer on hydrogen sensitivity and response time.

The second part of this work was dedicated to SAW-based hydrogen gas sensors fabricated on GaN epitaxial layers grown on SiC substrates.

4.1   Circular HEMT sensor design

We previously proposed that a NiO and IrO$_2$ layers could be used for a thermally stable Schottky gate interfaces in AlGaN/GaN HEMTs [16]-[18]. The thermal stability of the gate interfaces is

[30] Y. Takagaki, et al., Guided propagation of surface acoustic waves in AlN and GaN films grown on 4H– SiC (0001) substrates, Phys. Rev. B 66 (2002) 155439

[31] P.V. Wright, Modelling and Experimental measurements of the reflection properties of SAW metallic gratings, proc. IEEE ultrason. symp. (1984) 54-63

[32] W. R. Smith et al., Analysis of Interdigital Surface Wave Transducers by Use of an Equivalent Circuit Model IEEE T Microw. Theory, MTT-17 (1969) 856-864

[33] C. K. Campbell, Surface Acoustic Wave Devices for Mobile and Wireless Communications, Academic Press, New York (1998) 126

[34] S.- H. Lee, et al., Epitaxially Grown GaN Thin-Film SAW Filter with High Velocity and Low Insertion Loss, IEEE T Electron. Dev. 48 (2001) 524-529

[35] R. C. Woods, F. A. Boroumand, Comments on "Epitaxially Grown GaN Thin-Film SAW Filter With High Velocity and Low Insertion Loss", IEEE T Electron. Dev., 53 (2006) 173-176

[36] X. Xu, R.C. Woods, On the piezoelectric coupling constant of epitaxial Mg-doped GaN, Solid-State Electron. 54 (2010) 680–684

[37] M. Clement, et al., SAW characteristics of AlN films sputtered on silicon substrates, Ultrasonics 42 (2004) 403–407

[38] Rýger, MEMS gas sensors based on SAW-HEMT structures, diploma thesis, Slovak University of Technology, 2011

[39] F. –Ch. Huang, Y. Y. Chen, T. T. Wu, A room temperature surface acoustic wave hydrogen sensor with Pt coated ZnO nanorods, Nanotechnology 20 (2009) 065501 doi:10.1088/0957-4484/20/6/065501

[40] W. Jakubik, et al., Bi-layer nanostructures of CuPc and Pd for resistance-type and SAW-type hydrogen gas sensors, Sensor. Actuat. B-Chem. 175 (2012) 255– 262

[41] C. Viespe, C. Grigoriu, SAW sensor based on highly sensitive nanoporous palladium thin film for hydrogen detection, Microelecton. Eng. 108 (2013) 218–221

[15] http://www.bureau.tohoku.ac.jp/kohyo/kokusai/06Feb3research-overview.htm [online] 18-march-2015

[16] T. Lalinský, G. Vanko, M. Vallo, E. Dobročka, I. Rýger, and A. Vincze, AlGaN/GaN high electron mobility transistors with nickel oxide based gates formed by high temperature oxidation. Appl. Phys. Lett., 100 (2012) 092105.

[17] I. Rýger, G. Vanko,P. Kunzo, T. Lalinský, M. Vallo, A. Plecenik, L. Satrapinski, T. Plecenik, AlGaN/GaN HEMT based hydrogen sensors with gate absorption layers formed by high temperature oxidation. Procedia Engn., 47 (2012) 518-521

[18] I. Rýger, G. Vanko, T. Lalinský, P. Kunzo, M. Vallo, I. Vávra, T. Plecenik, Pt/NiO ring gate based Schottky diode hydrogen sensors with enhanced sensitivity and thermal stability, Sensor. Actuat. B-Chem., 202(2014) 1-8

[19] Hudeish, A., Y. O., Gallium nitride (GaN) based gas sensor using catalytic metal , Thesis, Universiti Sains Malaysia, 2005

[20] H. Wipf, Solubility and Diffusion of Hydrogen in Pure Metals and Alloys, Phys. Scripta T94 (2001) 43-51

[21] G. Vanko, M. Vallo, T. Lalinský, and U. Heinle, in 9th International Conference on Nitride Semiconductors, Glasgow, 10–15 July 2011

[22] K. Wang, M. Ye, Parameter determination of Schottky-barrier diode model using differential evolution, Solid-State Electronics 53 (2009) 234–240

[23] Y.- T. Yan, Ch.-T. Lee, Improved detection sensitivity of Pt/β- Ga2O3/GaN hydrogen sensor diode, Sensor. Actuat. B-Chem. 143 (2009) 192-197

[24] G. Chen, J. Yu, P. T. Lai, A study on MIS Schottky diode based hydrogen sensor using La2O3 as gate insulator, Microelectron. Reliab. 52 (2012) 1660-1664

[25] T.-H. Tsai, et al., SiO2 passivation effect on hydrogen adsorption performance of a Pd/AlGaN-based Schottky diode, Sensor. Actuat. B- Chem., 136 (2009) 338–343

[26] J. Song et al., AlGaN/GaN Schottky diode hydrogen sensor performance at high temperatures with different catalytic metals, Solid State Electron. 49 (2005) 1330–1334

[27] J. Schalwig, et al., Gas sensitive GaN/AlGaN-heterostructures, Sensor. Actuat. B- Chem. 87 (2002) 425–430

[28] M. A. Salam, S. Sufian, Y. Lwin, and T. Murugesan, Hydrogen Storage of a Fixed Bed of Nanocrystalline Mixed Oxides, ISRN Nanomaterials Volume 2013, Article ID 539534, 10 pages

[29] D.C. Koningsberger, M.K. Oudenhuijzen, J.H. Bitter , The Nature of the Pt-H Bonding for Strongly and Weakly Bonded Hydrogen on Platinum : A XAFS Spectroscopy Study of the Pt-H Antibonding Shape Resonance and Pt-H EXAFS, J. Phys. Chem. B. 105 (2001) 4616-4622

achieved thanks to the NiO and IrO_2 naoncrystalline layers that can be formed by the thermal oxidation of Ni or Ir at 800°C in an oxygen atmosphere. In this work, we combine these layers with a Pt catalytic metal on top, and we propose that these stacks can be used for hydrogen absorption in an AlGaN/GaN HEMT gate diode sensor.

For the hydrogen sensor, we designed a high electron mobility transistor with circular gate topology (C-HEMT) (Fig. 4.1.) This topology does not require any mesa-etching to isolate the devices. The C-HEMT ring gate diode can be easily patterned, and the gate leakage current is significantly suppressed because of the absence of the gate current tunnelling effects, which often occur at mesa-etched edges in conventional rectangular HEMTs.
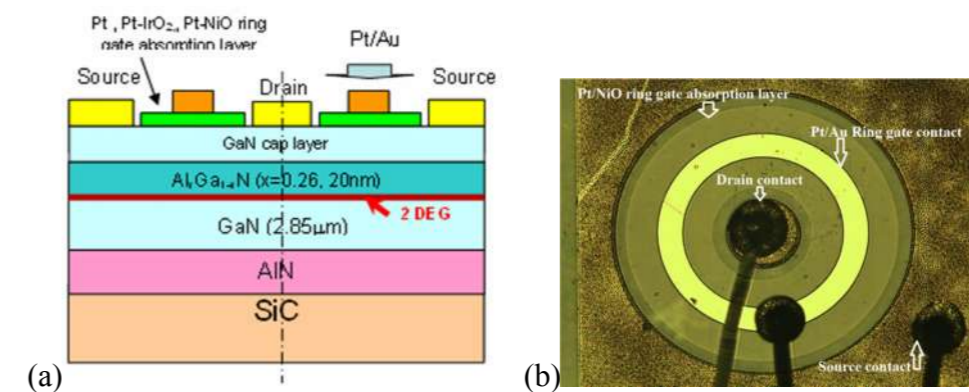

Fig. 4.1. The C-HEMT sensor device cross-section (a) and the ring electrode layout –fabricated structure top view (b).

Transistor ohmic contacts were based on Nb-Ti-Al-Ni-Au stack and were alloyed at 850°C. The Ni and Ir ring gate contacts of variable thickness (5, 10 and 15 nm) were formed by the electron beam evaporation and lift-off technique. Then the thermal oxidation of the Ni or Ir gate contacts was performed in an O_2 ambience using rapid thermal annealing (RTA) at 800°C for 1 min. This transformed the entire Ni and Ir gate layers into their crystalline oxides NiO and IrO_2. This process gave the gate interface better stability at elevated temperatures [17]. Moreover, these additional layers serve as a diffusion barrier for the following gate contact.

Metals that are suitable for the gate absorption layer have a partially-filled d orbital whose electrons are involved in the chemisorption bonds [19]. Moreover, the solubility and diffusivity of a particular gas through the absorption layer plays an important role in the sensory mechanism [20]. Therefore, we used a 15 nm-thick Pt catalytic absorption layer for the transistor top gate layer.

4.2 Gate absorbing layer microstructure and morphology

The NiO and IrO_2 layers formed by high temperature oxidation have nanocrystalline structure. This allows easier hydrogen diffusion through nanocrystal grain boundaries. Moreover, the raising surface roughness increases the absorption area what relates to the efficiency of adsorption process [18]. To investigate the microstructure of gate absorbing layer, we used atomic force microscopy (AFM) and transmission electron microscope (TEM) cross-section view. First, a 10-nm thick Ni metal layer was deposited on AlGaN surface. Then it was annealed in oxygen ambience at several temperatures. This

sample was then subjected to TEM analysis. The TEM cross-section shows that the thickness of the NiO layer is about twice as that of the as-deposited Ni layer (Fig. 4.2. (b)). Also, it is evident that the Ni layer completely transformed into its oxide through to the AlGaN interface. One can also notice that the NiO single grain size determined the thickness of the oxide layer. Please note that many mechanical defects (cracks) appear on the surface of epitaxial AlGaN layer.
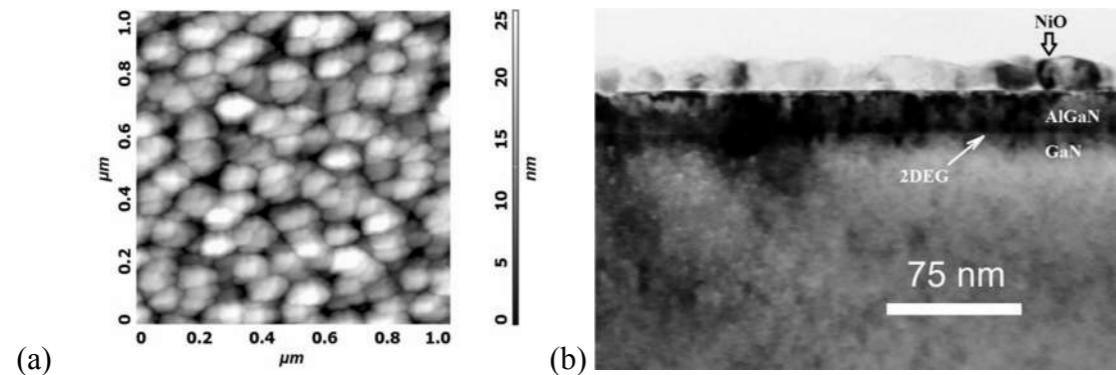

Fig. 4.2. AFM surface morphology (a) and TEM cross-section view (b) of NiO/AlGaN/GaN stack formed at 800°C.

The TEM analysis of the gate stack corresponds with the x-ray diffraction (XRD) analysis that was performed for thermic NiO gates of AlGaN/GaN HEMTs [16]. The XRD analysis of the gate layers revealed the NiO phases in the gate layers showed a strong orientation preference, similar to that of epitaxial layers [21].

4.3   Schottky diode current-voltage characteristics

To see the effect of additional oxide layers on Schottky junction transport parameters, the current-voltage measurements were performed. The Schottky diode characteristics measurements were performed on HP4145 semiconductor parameter analyser.
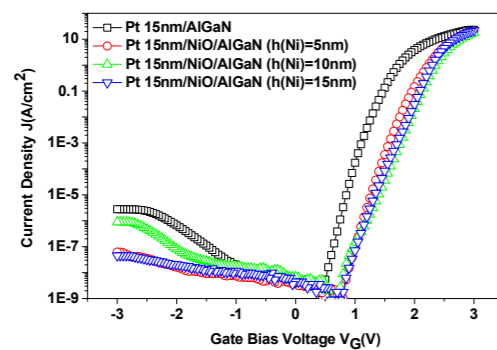

Fig. 4.3. Electrical I-V characteristics of Schottky diodes with varying thickness of NiO layer.

Bias voltage was swept from 3V downwards to -3V with step 0.05V and the integration time was set to medium (64-times power line cycle) in order to suppress the noise background of measurements. Measurements were carried out either with light background or without sunlight. There was no noticeable shift by photogenerated current in reverse direction. It is shown that with the increasing thickness of NiO the diode saturation current considerably decreases. In the reverse direction, the introduced layer suppresses the leakage current.

was about 20 ppm. Moreover, the sensor reaction time constant at 1000 ppm H_2/N_2 reached value of 12 s. So it is suitable for fast on-line gas analysis systems based on sensor arrays.

6   References

[1]   V. Cimalla, J. Pezoldt, O. Ambacher, Group III nitride and SiC based MEMS and NEMS: material properties, technology and applications, J. Phys. D: Appl. Phys. 40 (2007) 6386–6434

[2]   http://en.wikipedia.org/wiki/Gallium_nitride [online] 31-march-2015

[3]   O. Ambacher, et. al., Two-dimensional electron gases induced by spontaneous and piezoelectric polarization charges in N- and Ga-face AlGaN/GaN heterostructures, J. Appl. Phys., Vol. 85, No.6 (1999), 3222-3233

[4]   J. Song, et- al., Pt-AlGaN/GaN Schottky diodes at 800°C for hydrogen sensing, Appl. Phys. Lett. 87, 133501 2005

[5]   J. Song, et al., Operation of Pt/AlGaN/GaN- Heterojunction Field-Effect-Transistor Hydrogen Sensors With Low Detection Limit and High Sensitivity, IEEE Electr. Device. L. 29 (2008) 1193-1195

[6]   T- Lalinsky, I. Rýger, L. Rufer, G. Vanko, Š. Haščík, Ž. Mozolová, M. Tomáška, A. Vincze, F. Uherek, Surface Acoustic Wave Excitation on SF6 plasma treated AlGaN/GaN heterostructure, Vacuum, 84 (2009) 231-234

[7]   I. Rýger, et al., An AlGaN/GaN based GHz-range surface acoustic wave oscillator for sensor applications, Proc. 22nd Inter. Conf. Radioelektronika 2012. Eds. R. Balada et al. Brno: Univ. Technol. 2012. ISBN 978-80-214-4468-3. P. 279-282

[8]   Rýger, I., Vanko, G., Lalinský, T., Vallo, M., Tomáška, M., Ritomský, A., AlGaN/GaN based SAW-HEMT devices for chemical gas sensors operating in GHz range. Procedia Engn. 25 (2011) 1101-1104.

[9]   I. Lundström, M. S. Shivaraman, C. Svensson, and L. Lundkvist, Appl.Phys. Lett. 26 ,55 (1975)

[10]   Y. Irokawa, Hydrogen Sensors Using Nitride-Based Semiconductor Diodes: The Role of Metal/Semiconductor Interfaces, Sensors 11 (2011) 674-695

[11]   J. Yu, et al., Hydrogen gas sensing properties of Pt/Ta2O5 Schottky diodes based on Si and SiC substrates, Sensor. Actuat. A-Phys. 172(2011) 9-14

[12]   K. Matsuo , et. al., Pt Schottky Diode Gas Sensors Formed on GaN and AlGaN/GaN Heterostructure, Appl. Surf. Sci. 244 (2005) 273-276

[13]   H. Hasegawa and S. Oyama, J. Vac. Sci. Technol. B 20 (2002) 1647

[14]   D. S. Ballantine, R. M. White, Acoustic Wave Sensors. Theory, Design and Physico-Chemical Applications, Academic Press, 1997, pp. 72, 80

showed a larger peak Schottky barrier height lowering of 0.2 eV, contrary to that of the reference sensor which shows 0.11 eV in peak. The application of hydrogen increased the contribution of thermionic emission to the forward current transport mechanism. Thus, we observed that the diode ideality factor decreased by 0.6 and 0.7 for the reference sensor and the sensor with oxide layer, respectively.

The transient characteristics showed that the sensor reaction and the regeneration time of the sensor with NiO were deteriorated by a longer diffusion path towards the semiconductor interface. Therefore, the reaction time constant τ_{R1} of the proposed sensor was 2.4-times higher than that of the reference sample (50°C, 200 ppm H_2/N_2). This corresponds to the reaction time constants of 600 s and 250 s for the sensor with NiO and the reference sensor, respectively. At a higher hydrogen concentration (1000 ppm) and an elevated temperature (above 100°C), this difference decreased and the reaction time constants for both reference and oxide-based sensor were comparable.

The introduced Pt/NiO gate diode sensing layer could rank among the metal-oxide-semiconductor (MOS) diode structures with a great potential for hydrogen monitoring in harsh environments and anaerobic conditions.

GaN/SiC based SAW hydrogen sensor was investigated in the second part of this work. We showed that decrease of acoustic wavelength and mechanical energy confinement in epitaxial waveguide improves the surface mass-loading sensitivity. About 10% change of group velocity is observed on structures with period 4 μm. These structures showed also the highest electromechanical coupling of 3.5%, what is desirable for low-loss SAW filters. We also showed that first order *Rayleigh-like* mode is especially suitable for gas-sensing purpose due to efficient confinement of acoustic wave energy close to surface. However, it has been shown that there is large discrepancy between K^2-measurement methods. This was attributed to leaky nature of SAW generated in layered media. Consequently, the transmission-based methods give, in general, lower K^2 values due to elastic wave power loss into bulk material. Therefore, for given material system GaN/SiC with piezoelectric GaN layer of the thickness of 1.7 μm, the solid-electrode transducer seems to be better alternative due to its large electro-mechanic coupling and shorter achievable SAW wavelength resulting in higher mass sensitivity than that of its split-electrode alternative. On the other hand, the triple transit echo signals are efficiently suppressed using split-electrode transducers.

Finally, the SAW sensor was used in feedback loop of delay-line microwave oscillator. The sensor was tested at room temperature in nitrogen ambience. We showed that hydrogen concentration-dependent oscillator frequency shift is linearly dependent on logarithm of hydrogen concentration, what makes these sensors suitable for analytic purpose. Measured sensor response showed large frequency shift (more than 60 kHz) upon exposure to 1000 ppm H_2/N_2. The sensor detection limit

A careful reader can particularly notice an interesting shift of zero-current point noticeable in Fig. 4.5 which would lead us to false conclusion that the diode acts as an autonomous voltage source. This effect appears only at diodes with very low saturation current densities. It is caused by effect of parasitic junction capacitance connected in parallel to ideal Schottky contact. If the ramp voltage falls down (in the case of measurement from maximum forward positive bias voltage to negative reverse bias), the capacitive current has negative value. This capacitive current adds to the diode conductive current (that is positive in forward bias). Consequently, there exists a point, where these two currents equal in value, but have opposite direction. This leads to creation of virtual zero current crossing point. If the voltage higher than this virtual „zero current voltage" is applied, the conductive junction current will dominate. On the other hand, the capacitive current dominates in region of small forward and reverse voltages.

4.4   Differential evolution algorithm for Schottky barrier height estimation

To quantitatively evaluate the influence of the additional oxide layers and hydrogen on Schottky barrier contact, as well, we used a differential evolution non-linear curve fitting algorithm. This stochastic optimization method [22] has come as an alternative to classical genetic algorithm and simulated annealing algorithm. An important advantage of this method is that the initial guess close to solution is not required. In contrast, the parameter determination problem can be based on broad range specified for each parameter. This method borrows the Nelder-Mead's method and employs the random generated initial population, differential mutation, crossover probability and greedy-criterion based selection to find minimum of the error function. This method extracts the distance and direction information from current population of solution to guide further search. This method needs very little information about problem; it has simple structure and fast convergence speed. Thus, it is convenient to solve complex optimization problems.

The differential evolution creates a random population and generates new offsprings (trial vector) of each parent individuals (target vector) of the population. The trial vector is generated by means of statistical mutation and crossover. First, the mutation operator creates the mutant vectors by adding the extracted distance and direction information from the current population members to another individual. Using crossover operator, the mutated vector components are consequently mixed with components of another vector. The selection process replaces the predetermined population member by the generated offspring, if it has lower error function value. If the predetermined criteria are met or maximum number of passes has reached, the algorithm will end.

Using this method, we created algorithm in Matlab code run on GNU Octave M-code interpreter. The algorithm is described in Appendix D in this dissertation. An example of Schottky barrier height determination from experimental data (cross-symbol) using abovementioned algorithm is shown in Fig. 4.4. It also documents fast convergence of proposed algorithm.
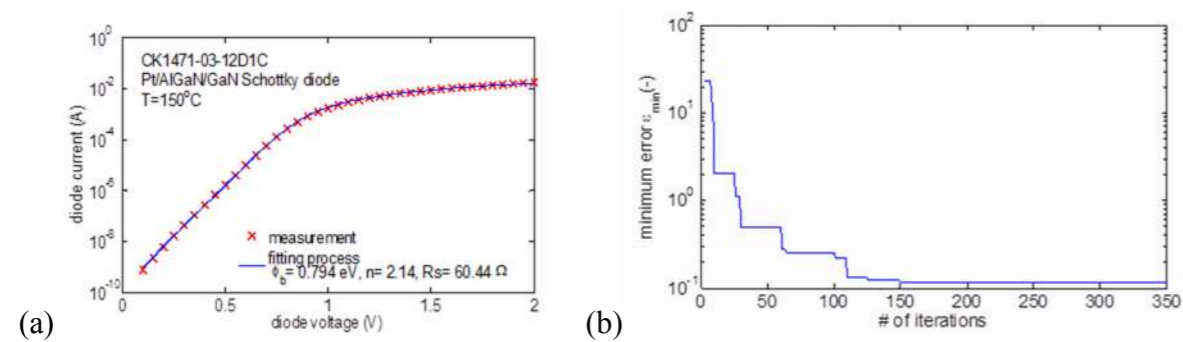
(a)   (b)

Fig. 4.4. Schottky barrier height estimation algorithm result (a) and the algorithm speed of convergence (b).

Gas sensing experiment

Next, the sensor was placed in stainless-steel gas test chamber of approximate total volume 125 cm^3. The chamber was heated by boron-nitride ceramic heater. Hydrogen mixture with nitrogen carrier gas were used for sensor testing and the precise concentration was regulated by mass-flow controllers The total gas pressure was 1 bar. The volumetric flow rate was set to 125 cm^3/min. First, the gas chamber was purged by nitrogen for 10 minutes. Then, a mixture of hydrogen in nitrogen carrier gas with concentration 1000 ppm was applied for 10 minutes. Finally, the chamber was purged for 10 minutes with nitrogen gas. At the end of each period, the sensor characteristics were measured.

To evaluate the sensing response of the sensor, we defined the response function (SF) as a relative change in diode current with (I_{H2}) and without hydrogen applied (I_0). This response function was evaluated for each bias value within the bias voltage interval.

4.5   Static characteristics

4.5.1   Pt/AlGaN/GaN diode hydrogen sensor

The characteristics of Pt/AlGaN/GaN diode gas sensor were subjected to 1000 ppm H$_2$/N$_2$ peak measured at various temperatures ranging from 50°C up to 500°C as the observable gas sensing response appeared at 150°C (Fig. 4.5. (a)).

From measured I-V characteristics, we can plot the sensitivity function dependence on bias voltage. We found that the Pt/AlGaN/GaN sensor has peak sensitivity, when it is forward-biased and the optimum bias voltage slightly shifts with varying temperature (Fig. 4.5. (b)). The optimum bias voltage is around 0.4-0.6V and the shift of maxima can be attributed to the fact, that sensitivity at large diode current is decreased due to voltage drop on the diode series resistance.

twice shorter SAW wavelength than with the other type of transducer. This resulted in a higher effective waveguide aperture and better acousto-electrical SAW excitation.

4.11   SAW sensor testing

For investigation of sensory characteristics of proposed sensor, a feedback-loop delay line travelling wave oscillator was employed. This concept requires a simple data acquisition system based on digital frequency counter. The delay line oscillator concept was investigated in our previous work[7][38]. Hydrogen in mixture with nitrogen carrier gas was used to test the performance of our device. Similar measurement procedure was used as in the case of HEMT gate sensors. Rising hydrogen gas concentration steps were applied to SAW sensor and the time-dependent oscillator frequency shift was recorded.
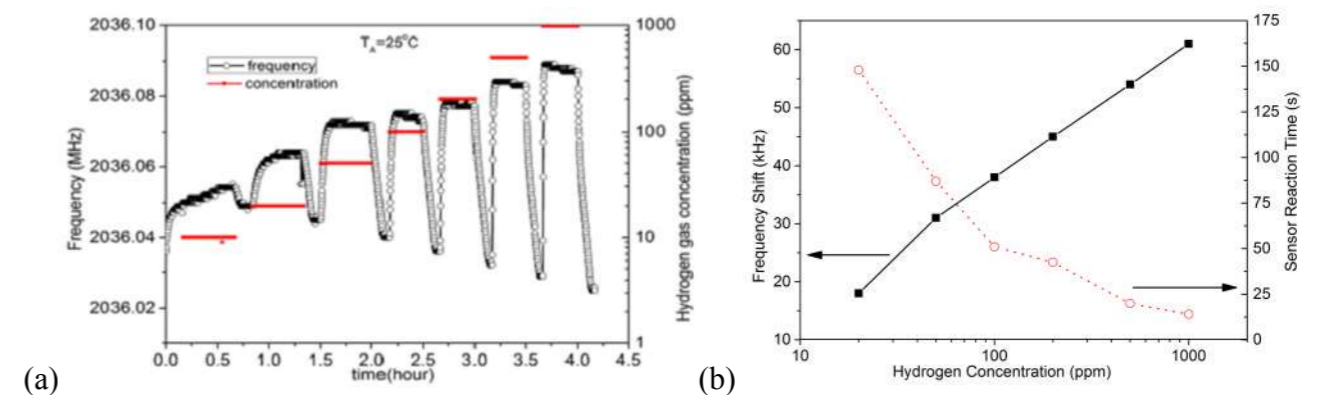

(a)   (b)

Fig. 4.16. SAW sensor response to hydrogen concentration steps (a) and extracted frequency shift and reaction time (b).

The sensor response to a concentration step is depicted in Fig. 4.16.(a). We note that the sensor signal is linearly dependent on logarithm of hydrogen concentration (Fig. 4.16. (b)). This is a particular advantage for wide-range analytic gas detectors. The maximum frequency deviation upon exposure of 0.1% H$_2$/N$_2$ reached a value of 60 kHz. Accordingly, this sensor can rank among the high-sensitivity hydrogen SAW sensors operating at room temperature [39]-[41].

5   Conclusions

The first part of this dissertation reports on the application of a new gate absorption layer based on a nanocrystalline gate oxide Pt/NiO or Pt/IrO$_2$ stacks for a HEMT or Schottky diode-based hydrogen gas sensors. The presence of the semi-conducting oxide layer increased the effective Schottky barrier height, which is desirable for sensors that are operated at high temperatures. The static and dynamic response of the Schottky diode hydrogen sensors with this new type of chemical absorption layers is investigated. The sensory properties of this device are compared with those of a reference Pt/AlGaN/GaN sensor. Especially by virtue of the nanocrystalline structure of NiO, the low temperature response of the Pt/NiO/AlGaN/GaN sensor was increased 60-times, compared with that of the reference sensor (50°C, 1000 ppm H$_2$/N$_2$). This additional layer provided many more oxygen absorption sites for hydrogen, and it also served as a sorbent. Thus, the sensor with NiO layer

In our work, we compared the calculated values of K^2 from our measurements using several approaches. The results are summarized in Tab. 4.1.

Tab. 4.1. Comparison of electromechanical coupling factors determined by four different methods.

Solid-Split electrode/ IDT period (Λ)	Synchronous Frequency f_0(GHz)	K^2_{eff} (%) Method [33]	K^2_{eff} (%) Method [35]	K^2_{eff} (%) Method [37]	K^2_{eff} (%) Method [36]
Solid/ 3.2µm	2.038	2.16	3.103	0.349	0.313
Solid/ 3.2µm	2.037	2.32	2.93	0.411	0.331
Solid/ 4 µm	1.704	2.87	3.561	0.524	0.569
Solid/ 4 µm	1.705	2.87	3.513	0.452	0.442
Split/8 µm	0.956	0.882	0.362	0.0557	0.00351
Split/8 µm	2.366	0.96	0.563	0.0318	--
Split/8 µm	0.945	0.64	0.287	0.0381	0.0494
Split/8 µm	2.356	0.76	0.33	0.0621	0.124

As seen from the calculated values, in our case the first method yielded physically larger values of the electromechanical coupling, compared with the second method. Finite element transient simulations of the GaN/SiC-based SAW devices showed that a certain amount of energy was also transported in SiC substrate (that is piezoelectrically inactive) in the form of leaky waves (Fig. 4.15.) [37].
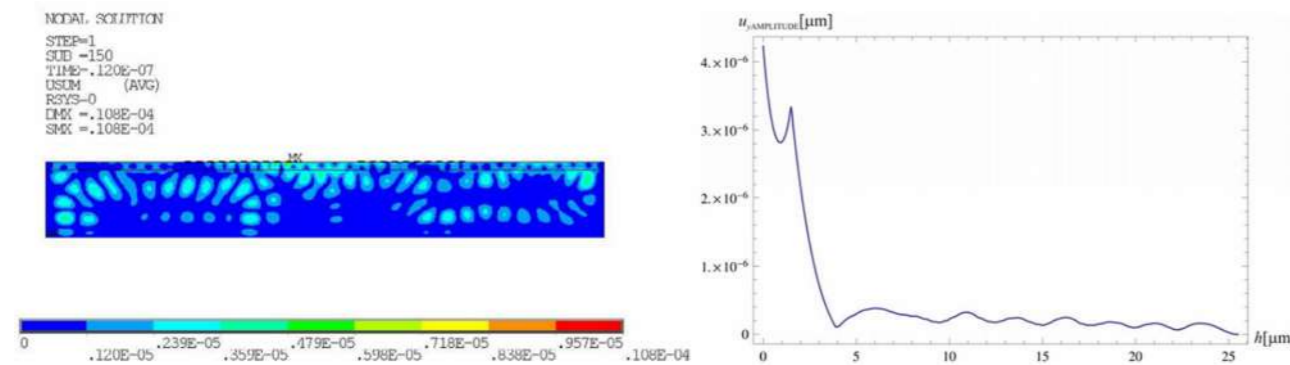

Fig. 4.15. 2D profile of SAW elastic deformation (a) and depth profile of transverse displacement (b).

Therefore, a reduced amount of strain energy reached the output transducer. As a consequence, the values of the electro-mechanical coupling factor obtained from the transmission measurement are lower than those obtained from the reflection coefficient measurements.

In general, the solid-electrode IDT provided an advantage of a stronger electro-mechanical coupling if compared with its split-electrode counterpart. With the first type of transducer, one can achieve a
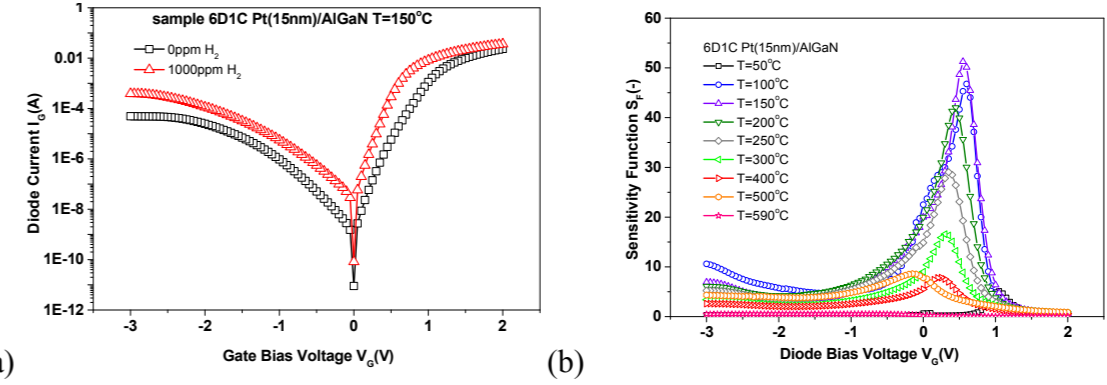

(a)   (b)

Fig. 4.5. I-V characteristics of Pt/AlGaN/GaN Schottky diode gas sensor measured at 150°C(a) and gas response bias dependence (b).

When the temperature is increased, the thermionic emission current rises. Consequently, the series resistance-limited current region shifts toward lower bias voltages. On the other hand, the sensitivity in low-current region is probably affected by non-ideal effects like tunneling. From this sensitivity peak maxima (Fig. 4.5. (b)) at various temperatures, we obtained its temperature dependence. With rising temperature the sensitivity first increased and showed the peak at apparent optimum working temperature 150°C. Then the relative sensitivity decreased. This imaginary optimal temperature was caused by slow sensor response at low temperature (the measurement was performed before the stabilization of sensor signal).

4.5.2 Pt/AlGaN/GaN HEMT hydrogen sensor

When the gas sensor was operated in HEMT transistor mode, the drain and gate bias voltages were applied to inner circular ohmic contact and Schottky gate ring electrode, respectively. The outer ohmic contact was used as a source contact in order to minimize the parasitic source resistance. The source electrode was grounded. Fig. 4.6. (a). shows the transfer characteristics of HEMT gas sensor. We can see a clear shift of the threshold voltage.
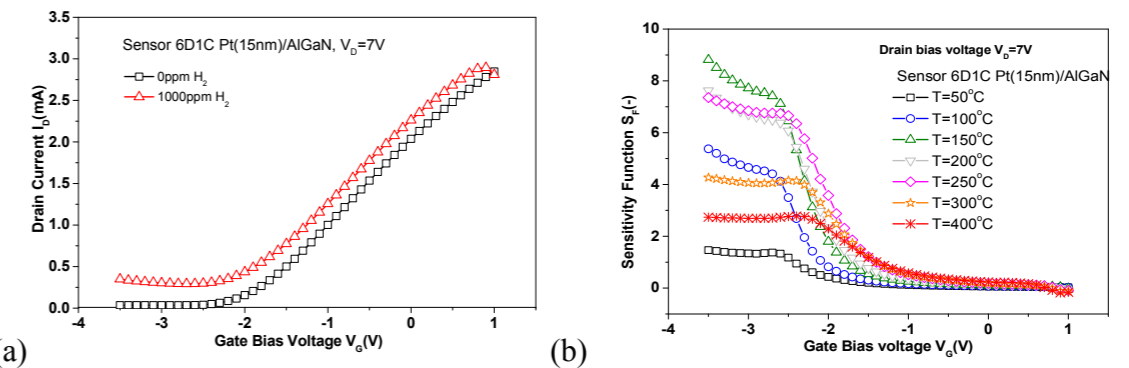

(a)   (b)

Fig. 4.6. The Pt/AlGaN/GaN HEMT sensor transfer characteristics (a) and bias dependence of gas sensitivity (b).

Moreover, in the sub-threshold region, the current starts flowing through channel. It is caused by increased reverse current of Schottky contact due to application of hydrogen gas. From the transfer characteristics at various temperatures, the bias dependence of sensitivity was obtained (Fig. 4.6. b). It can be seen that maximum sensitivity function in the sub-threshold region is also observed at working temperature of 150°C in accordance with that of Pt/AlGaN/GaN diode sensor. Provided that

sensitivity peak around threshold voltage is not observed in transfer characteristics, the effect of gas application on 2-DEG density is overbuilt by more intense Schottky diode reverse current change.

4.5.3 Pt/NiO/AlGaN/GaN diode sensor

Schottky diode measurement was also performed on device with nanocrystalline NiO layer between Pt Schottky metal and AlGaN (Fig. 4.7.(a)). Both sensors with 5nm and 15nm thick initial Ni layer (being transformed into NiO) show large sensitivity to hydrogen gas. Moreover, we observed distinctive change in diode reverse current characteristics after exposure to hydrogen.

(a)   (b)
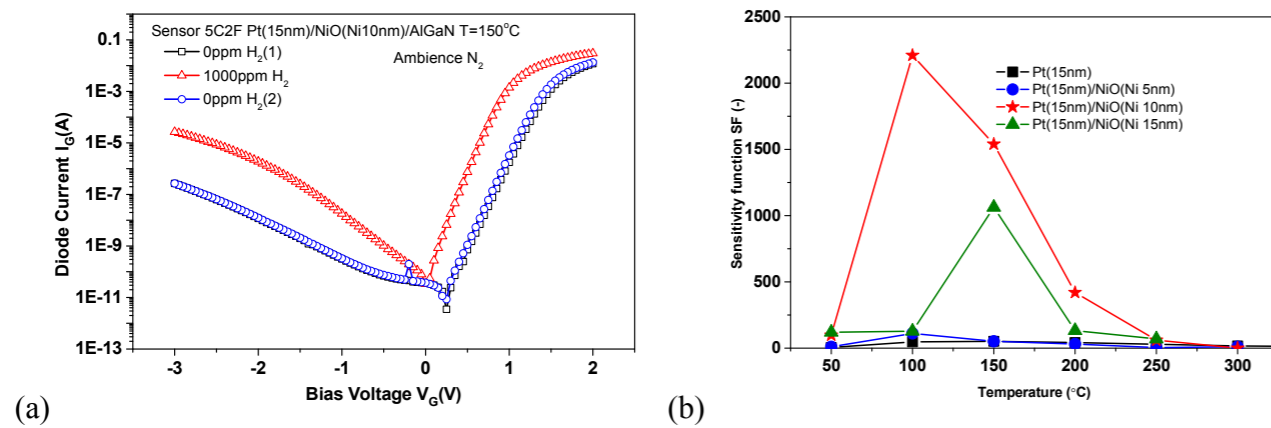
Fig. 4.7. I-V characteristics of NiO based diode sensors upon exposure to hydrogen applied in nitrogen (a) and response function for sensors with different NiO thickness as a function of temperature (b).

The device with NiO (Ni thickness of 10nm) exhibited the best hydrogen sensing response (Fig. 4.7. (b)). When comparing to standard Pt/AlGaN/GaN device, the sensitivity of proposed sensor is 43-times higher. We can clearly see that diode baseline saturation current (without hydrogen) of diode with NiO is about of 3 orders smaller, than that of sensor without NiO. This implies elevated Schottky barrier. Also the reverse current at high reverse bias shows the distinctive increase upon exposure to hydrogen.

Again, we observed the apparent peak response at temperature from 100 to 150°C. This virtual peak shifts towards higher temperatures, when the NiO thickness rises. The simple explanation is again due to finite measurement time (that is 10 min), so the sensor signal was not measured in steady state. Here, the increased thickness of NiO layer causes longer diffusion time of hydrogen through this layer. The diffusion process speeds up as the temperature rises, so the sensor reaches its steady-state value in shorter time. Therefore, the sensor response first "virtually" rises with increasing temperature. The maximum sensing response was obtained with sample NiO (10nm Ni). It showed almost 2250-times large current variation upon exposure to 1000ppm H_2/N_2.

The split-electrode transducers with period 8 μm have very small effective waveguide aperture. For this reason, the effective electromechanical coupling factor of these structures is low. Consequently the passband attenuation is high and the phase measurement of weak signals becomes very inaccurate. However, we can still clearly see that the mass-loading effect is much weaker (Fig. 4.13.(b)) than that of solid-electrode transducers. It is only about -2.8%. Therefore, we demonstrate that the twofold reduction of acoustic wavelength leads to considerable increase (about 3.7-times) of device mass sensitivity.

4.10 Effective electromechanical coupling factor measurement

The unified methodology for the extraction of this physical quantity has not been established yet. From its basic definition, the electro-mechanical coupling can be calculated from the relative difference of a SAW phase velocity on free and electrically-shortened surfaces. However, it is difficult to fabricate an infinitely-thin perfect conductor that would create an equipotential area on the crystal surface. Any deposited metal imposes due to its finite specific mass a certain error caused by surface mass-loading. Therefore, two main methods have been developed to determine this quantity. One method is based on the measurement of the transducer input reflection coefficient. The coupling factor can be determined from a closed-form formula derived from an equivalent circuit model [32]-[34] by taking the ratio between the real and imaginary parts of the transducer input admittance. A refined approach that compensates for the effect of parasitic stray impedances is based on the reflection coefficient dip [35]. Typical plots of the input reflection coefficient for both solid and split-electrode IDTs are shown in Fig. 4.14.
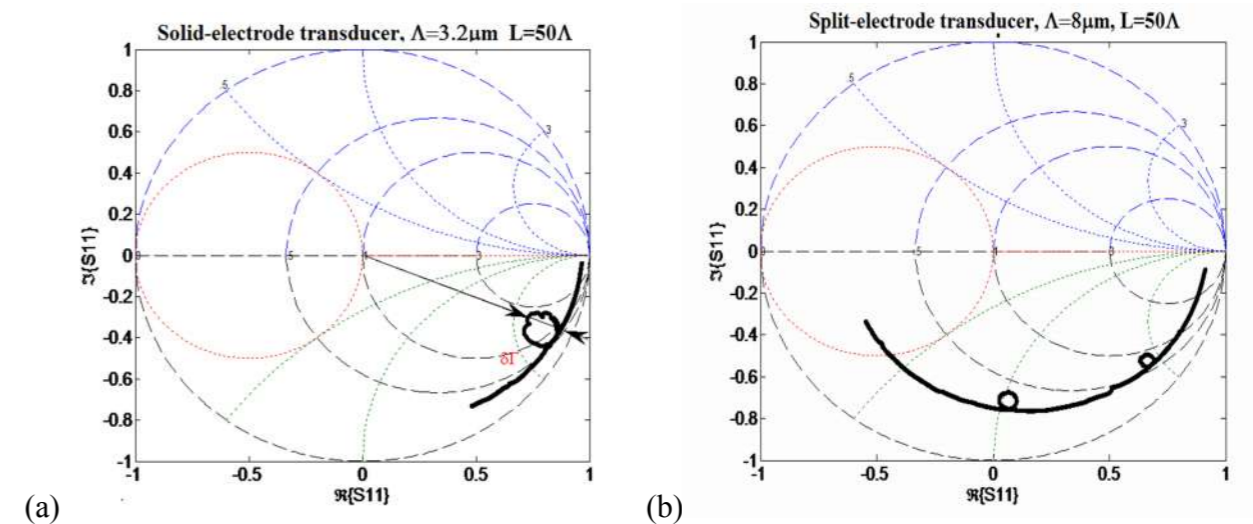

(a)   (b)

Fig. 4.14. Input reflection coefficient of solid (a) and split (b) electrode transducers.

The second method is based on either SAW device passband attenuation [36] or equivalent trans-admittance measurement [37]. Considering a bi-directional transducer, when no energy leakage occurs (due to leaky waves), the half of elastic power should reach the output transducer. Then the magnitude of measured trans-admittance is proportional to the electro-mechanic coupling factor.

velocity. Therefore, the mass-loading effect can be observed by measurement of the group velocity on free surface and the surface covered in the absorbing layer. To investigate the mass-loading effect, we measured the group delay of several SAW delay lines with varying propagation path length.

First, we measured the solid-electrode transducers with two different IDT periods. As expected, the group velocity for R2 mode decreases from 6374 m.s⁻¹ to 5633 m.s⁻¹ on free surface as the wavelength is shortened from 4 to 3.2 μm (Fig. 4.12.). The group velocity also decreases if the free surface is covered by 100 nm-thick Pd-metal. Structures with wavelength 4 and 3.2 μm show this velocity decrease from 6374 to 5716 m.s⁻¹ and from 5633 to 5353 m.s⁻¹, respectively. This implies the influence of mass-loading effect by more than 10 % in sample with 4 μm wavelength. It is interesting that the samples with wavelength of 3.2 μm show substantially lower mass-loading (only about 5 %).
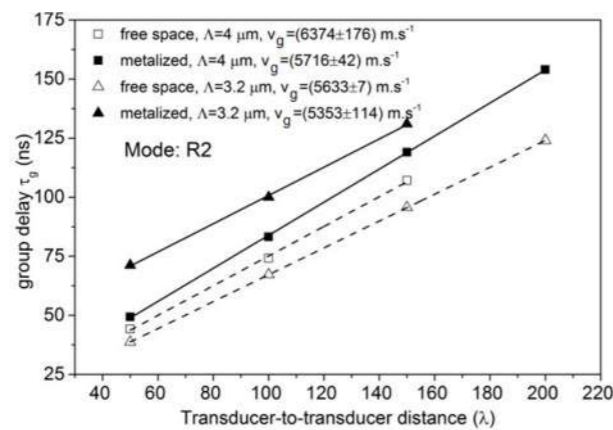

Fig. 4.12. Group velocity measurement of R2-mode on solid-electrode transducers with different period.

Likewise, the similar measurement was performed for split-electrode samples with larger acoustic wavelength and excited fundamental acoustic mode R1 (Fig. 4.13.(a)).
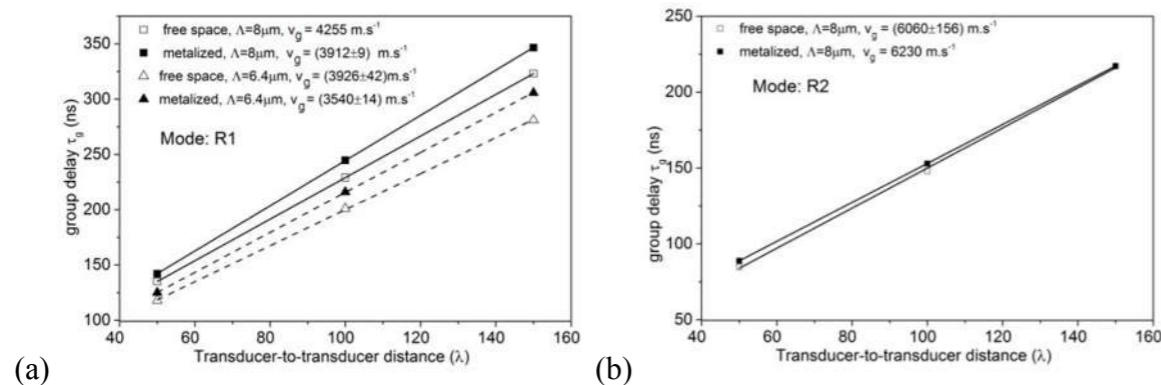

Fig. 4.13. Group velocity measurement of R1 (a) and R2 (b) mode in split-electrode transducer.

Here, at the same conditions the samples with deposited metal show velocity decrease from 4255 to 3919 m.s⁻¹ and from 3926 to 3540 m.s⁻¹ for wavelength 8 and 6.4μm, respectively. It shows the increase of mass-loading from 7.8 to 9.8 % as a wavelength decreases.

4.6 Schottky barrier height evaluation

To elucidate the hydrogen sensing mechanism, the Schottky barrier height variation and the ideality factor change as functions of temperature and applied hydrogen gas were extracted (Fig. 4.8.). We used above mentioned fitting algorithm based on a differential evolution [22]. The simple thermionic emission model was applied in our approach [18]. It is described by Eq.(4.1) in which symbols I_{H2} and I_s denote the diode current upon the application of hydrogen and the saturation current, respectively. $\Delta\varphi_B$ and Δn represent the Schottky barrier height and the ideality factor lowering. The bias voltage applied across the Schottky barrier diode is represented by symbol V_G. The term q/kT represents the reciprocal thermal energy of electron in volts.

$$I_{H2} = I_S \cdot \exp\left(\frac{-q(\Phi_B - \Delta\Phi_B)}{kT}\right)\left(\exp\left(\frac{qV_G}{(n-\Delta n)kT}\right) - 1\right) \qquad (4.1)$$

One can see that the application of hydrogen affects the effective Schottky barrier height but it also modifies the value of the diode ideality factor (Fig. 4.8.). The Schottky barrier height and ideality factor decreased with the operation temperature under hydrogen application.
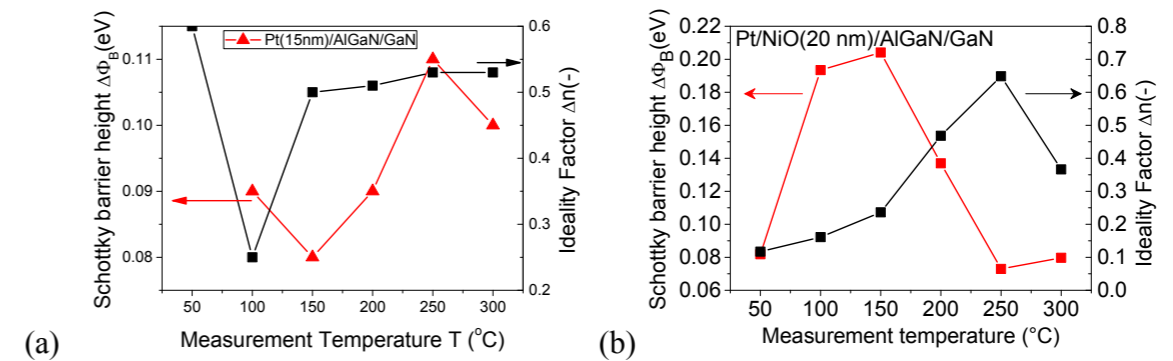

(a)　　　　　　　　　　　　　　(b)

Fig. 4.8. Schottky barrier height and ideality factor lowering of reference sensor (a) and sensor with NiO (b) exposed to hydrogen concentration of 1000 ppm as a function of operation temperature.

This effect was also observed in work [23].We can thus elucidate that the hydrogen induced dipole layer decreased the effective barrier height and improved the thermionic emission of electrons through the Schottky gate interface. This consequently increased the contribution of the thermionic emission to the diode current transport mechanism [10][24].

4.7 Sensor transient characteristics

In order to evaluate the sensor transient response, it was subjected to a continual flow of hydrogen in the carrier nitrogen gas [18]. The concentration of hydrogen was varied. The diode forward bias voltage was held constant and diode current was sampled periodically each 10 seconds. We chose the Pt-electrode gas sensor (Fig. 4.9. (a)) and sensor with Pt/NiO stack (Fig. 4.9.(b)) (NiO thickness 20nm, measured by TEM) for performance comparison. This was due to stable and reproducible transient characteristics among all tested sensors. As reader can see, the sensor response speeds up with rising hydrogen concentration. Obviously, the diode current follows two exponential curves.

After application of hydrogen it first rapidly grows and then it follows long exponential tail. The sensor baseline shifts gradually, what implies a long-term drift process. During the desorption process, the signal first rapidly decreases and then again slowly settles down. The sensor exponential does not reach its initial value (Fig. 4.9.) what shows that even after chamber purging, there is certain amount of hydrogen remnant in the sensor structure.
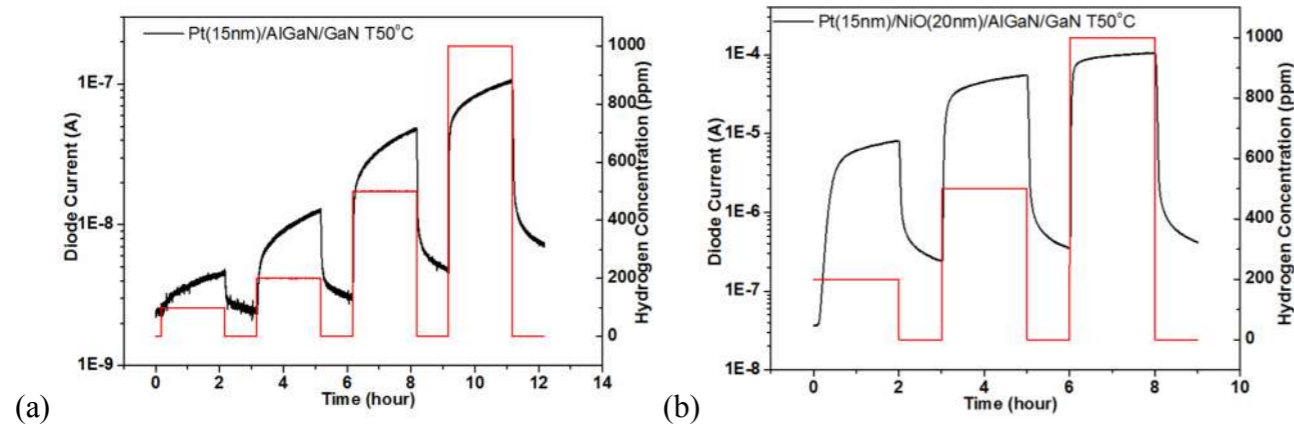

(a)   (b)

Fig. 4.9. Transient characteristics of sensor with Pt Schottky electrode (a) and Pt/NiO stack with NiO thickness 20nm (b).

The response functions of the both sensors were extracted from the measured transient characteristics at the end of the concentration step. As seen in Fig. 4.10., the presence of the oxide layer led to a considerable (60-times higher at 1000 ppm H_2) improvement in the sensor response at low temperatures (50°C) contrary to the reference sensor with flat Pt electrode [25]-[27], which exhibited the response peak around 250°C. The improved low temperature response of the Pt/NiO/AlGaN/GaN sensor is probably affected by the physisorption of hydrogen on the nanocrystalline surface of the stacked gate layer.
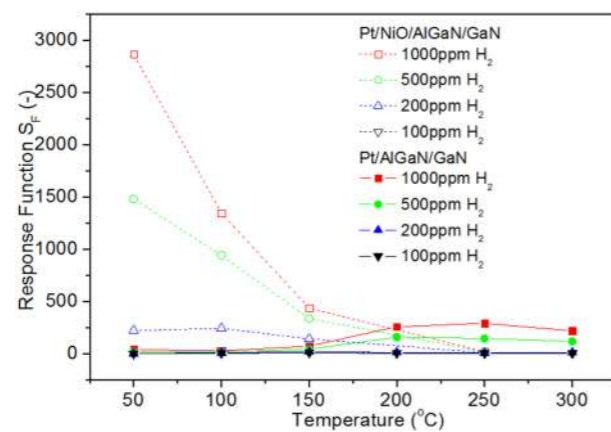

Fig. 4.10. Sensitivity of reference sensor (full symbols) and sensor with NiO (open symbols) obtained from time-domain measurements.

This layer acts as a sorbent, in which the hydrogen is bound by weak Van der Waals forces [28]. If the temperature rises, the energy of this weak attractive bond is surpassed by an increased thermal energy and the desorption overpowers the adsorption. Contrary to this, the bonding of hydrogen on flat Pt surface in the case of the Pt/AlGaN/GaN sensor is mainly governed by dissociative chemisorption [29]. Therefore, the sensor with the flat Pt surface has an increased response to the hydrogen gas at increased temperature, which is in agreement with [5].

4.8 SAW sensors

Our concept of SAW-based gas sensors follows the conventional arrangement with chemical absorption layer located between two interdigital transducers (Fig. 4.11.). The main difference from the ordinary sensor is to use the piezoelectric acoustic waveguide formed from epitaxial gallium nitride film grown on silicon carbide substrate. The phase velocity in bulk GaN crystalline material has value of 3693 m.s^{-1} , whereas in silicon carbide, it reaches 6832 m.s^{-1}[30]. This means that at the same frequency, the acoustic wavelength in GaN material is about twice shorter than in SiC. For this reason, it is expected that acoustic wave energy of excited Rayleigh-like modes will be confined within this epitaxial waveguide. Together with optimized interdigital electrode fabrication process (leading to shorter SAW wavelength), it will bring certain portion of elastic wave energy closer to the crystal surface and improved mass-sensitivity will be expected.
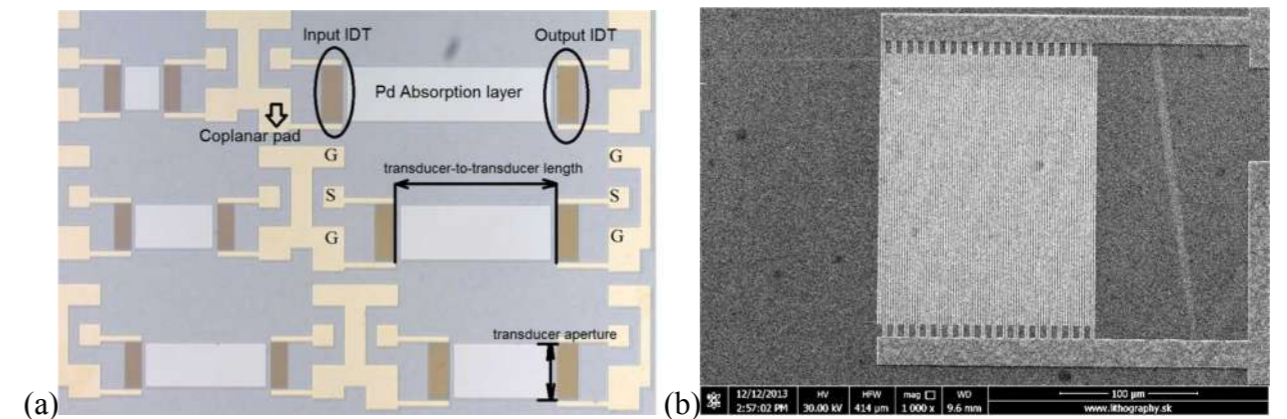

(a)   (b)

Fig. 4.11. Fabricated structures optical photograph(a) and scanning electron microscope detail of split-finger transcducer (b).

$Al_{0.25}Ga_{0.75}N$ /GaN heterostructure grown on SiC (0001) substrate was used for our experiments. This material was fabricated using MOCVD technology. The thickness of AlGaN barrier layer, GaN buffer and SiC substrate were 25 nm, 1.7 μm and 470 μm, respectively. Providing that 2-DEG (being formed at AlGaN/GaN interface) with high conductivity serves as an efficient electrostatic shielding layer, it would prevent the efficient generation of SAW. For this reason, our first experiments with SAW excitation on this material led to selective plasma treatment of the area under interdigital transducers. A shallow fluorine ion implantation should lead to depletion of 2DEG channel, but the SAW device insertion loss still remained very high [6]. For this reason, the AlGaN barrier layer was etched out (~50-100 nm) on the whole sample area. This process step ensured, that the SAW would be generated within the whole GaN layer [30].

4.9 Group velocity measurement

If the absorbing layer is deposited on top of the crystal, a certain amount of SAW elastic energy will be transported into this thin region. Therefore it affects the energy flow, and consequently, the group